Strong and Coherent Coupling between Localized and Propagating Phonon Polaritons

Christopher R. Gubbin,[1,2] Francesco Martini,[2] Alberto Politi,[2] Stefan A. Maier,[1] and Simone De Liberato[2]
[1]Department of Physics, Blackett Laboratory, Imperial College London, London SW7 2AZ, United Kingdom
[2]School of Physics and Astronomy, University of Southampton, Southampton, SO17 1BJ, United Kingdom
(Received 26 November 2015; revised manuscript received 23 February 2016; published 17 June 2016)

Following the recent observation of localized phonon polaritons in user-defined silicon carbide nanoresonators, here we demonstrate strong and coherent coupling between those localized modes and propagating phonon polaritons bound to the surface of the nanoresonator's substrate. In order to obtain phase matching, the nanoresonators have been fabricated to serve the double function of hosting the localized modes, while also acting as a grating for the propagating ones. The coherent coupling between long lived, optically accessible localized modes, and low-loss propagative ones, opens the way to the design and realization of phonon-polariton based coherent circuits.

DOI: 10.1103/PhysRevLett.116.246402

Surface phonon polaritons are surface-bound, propagative modes arising from collective oscillations of ions at the surface of polar crystals, analogous to surface plasmon polaritons on metallic surfaces [1,2]. When the surface is properly patterned, it can sustain also localized surface phonon polaritons, confined in extremely subwavelength volumes and characterized by quality factors and Purcell enhancements unparalleled in plasmonic systems [3,4]. Patterning, apart from creating the localized modes, also acts as a grating for phase matching to propagating surface polaritons [5], allowing us to tune their dispersion, and making it possible to bring them in resonance with the localized ones. The possibility to couple long lived localized resonances that can be resonantly pumped by an external source to low-loss propagative modes, with propagation lengths of hundreds of micrometers [6], hints to the tantalizing prospect to observe quantum effects in those systems, analogously to what was done with surface plasmon polaritons [7–9]. Moreover, the unique properties of phonon polariton resonators could lead to the realization of phonon-polariton based quantum circuits, overcoming the main problems hampering the development of quantum plasmonic circuits [10]. Here, using a silicon carbide (SiC) surface patterned by micrometer-sized cylinders, we demonstrate strong coupling between localized and surface modes by presenting clear evidence of spectral anticrossing, thus implying a coherent, reversible energy exchange [11,12]. Our work thus validates different building blocks toward a novel technological platform for coherent mid-infrared applications.

How tightly light of a given frequency may be confined is limited by the bandwidth of spatial frequencies available. The most famous example of this is the Abbe diffraction limit but the phenomenon is pervasive. Piecewise homogeneous material systems can sustain electromagnetic resonances localized around interfaces where the permittivity changes sign, the out-of-plane wave vector becoming imaginary and the bandwidth of spatial frequencies in-plane increasing. For a flat surface between air and a material with negative permittivity $\epsilon(\omega)$, this leads to surface modes characterized by the well-known dispersion

$$q = \frac{\omega}{c}\sqrt{\frac{\epsilon(\omega)}{\epsilon(\omega)+1}}, \tag{1}$$

where q is the in-plane wave vector and c is the speed of light. Surface plasmon polaritons are well-known surface modes in metals, whose Drude permittivity $\epsilon_D(\omega) = 1 - (\omega_P^2/\omega^2)$ becomes negative due to the coupling with collective plasma excitations in the region below the plasma frequency ω_P [13]. Strong field localizations are achievable in plasmonic systems, with good applications in waveguiding [14] and usually inefficient processes such as Raman spectroscopy [15]. Still, plasmons are inherently lossy [16], the modal energy spending half cycles as electron kinetic energy, leading to a dominant loss channel of electron-electron scattering occurring on the 0.01-ps scale [17], thus making it challenging to integrate them in quantum technology architectures [10,18]. As an alternative platform to metals, also polar dielectrics support surface polaritons in between the frequencies of the transverse optical phonon, ω_{TO}, and the longitudinal optical phonon, ω_{LO}, where the Lorentz permittivity $\epsilon_L(\omega) = [(\omega^2 - \omega_{\mathrm{LO}}^2)/(\omega^2 - \omega_{\mathrm{TO}}^2)]$ becomes negative as a result of light coupling to oscillations of the ions [19]. The damping of the ionic oscillations occurs on the 1-ps scale, 2 orders of magnitude slower than electron damping in metals. The resulting modes, called surface phonon polaritons [1], have been exploited for a number of applications, from enhanced energy transfer [20] and waveguiding [21] to thermal coherent infrared emission [22,23], superlensing [24,25], near field optics [26], enhanced optical forcing [27], and sensing [28]. More

exotic physics is expected in recently observed hyperbolic materials such as hexagonal boron nitride [29]. Analogously to localized plasmonic resonances, localized phonon resonances also appear in subwavelength dielectric systems. Mutschke [30] carried out explicit investigations into the infrared properties of small SiC particles of various polytype observing morphology dependent resonances analogous to particle plasmons. Subwavelength SiC whiskers have also been shown to support both localized electrostatic and propagative Fabry-Perot modes [3]. Recently, advances in fabrication procedures have allowed for the creation of user-defined cylindrical SiC nanoresonators on SiC substrate [4,31]. The modes exhibit quality factors exceeding the theoretical limit for plasmonic resonators. Moreover, while absolute confinement of light is less than in plasmonic systems due to the longer wavelengths involved, reducing potential nonlinear effects, relative confinement (in units of the wavelength) is comparable with the better plasmonic resonators [32], leading to Purcell enhancements 4 orders of magnitude greater than comparable plasmonic systems [4].

We used a 9.7 μm thick planar 3C-SiC layer grown over Si substrate, on which subwavelength cylindrical resonators of height $\simeq$800 nm and diameter $\simeq$1 μm were fabricated by ICP RIE in square 70×70 pillar arrays of varying periods from 5 to 7 μm. Numerical calculations show this depth of SiC is sufficient for convergence of reflectance measurements to those of bulk SiC, as can also be inferred from the inset in Fig. 1(a) where we see that the electric field of the surface mode in the dielectric is completely segregated into the SiC region. Full details on the fabrication can be found in the Supplemental Material [33]. The planar surface supports a surface mode whose dispersion, ω_q^s, is given by Eq. (1) with $\epsilon(\omega)$ the dispersive SiC dielectric function. While the surface polariton dispersion usually lies outside the light cone, the periodic patterning of the substrate results in a period-dependant band folding of the dispersion at the edge of the

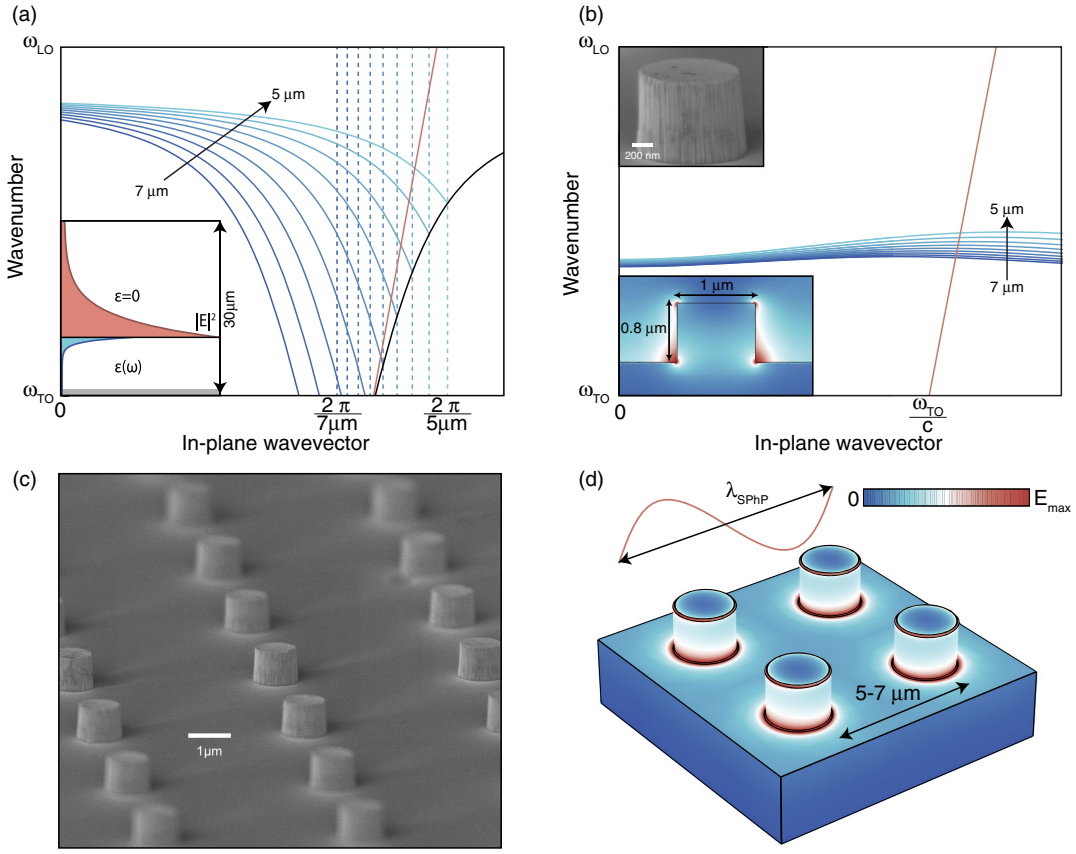

FIG. 1. (a) Fundamental dispersion of the surface mode is given by the black curve. Solid blue curves indicate surface mode folding from the edge of the first Brillouin zone (indicated by corresponding vertical dashed lines) for periodicities 5–7 μm. The red curve shows the vacuum light line. The inset shows the electric field norm for a surface mode at an air/SiC interface. The gray shaded region in the inset shows the beginning of the Si substrate on which the SiC wafer we used is grown, highlighting that the surface mode is almost entirely localized into the SiC region. (b) Tight-binding dispersion of the monopolar mode of a pillar array is indicated by blue curves for a variety of periodicities. The red curve is the vacuum light line, with c the speed of light. Insets show a slice of the mode electric field norm in an isolated SiC cylinder on substrate, calculated using COMSOL MULTIPHYSICS, and a SEM image of a fabricated resonator. (c) SEM image of the fabricated array. (d) Electric field norm for a mode of the coupled array. The sinusoid indicates the surface mode wavelength.

first Brillouin zone, as illustrated in Fig. 1(a), thus making them optically accessible. In the inset the electric field norm of a surface mode is plotted. The isolated cylinder-on-substrate system supports a number of modes as discussed in Ref. [31]. For the remainder of this Letter we will only consider the monopolar mode whose electric field norm is shown in the lower inset of Fig. 1(b). This mode is a longitudinal mode of the cylinder mediated by the substrate resulting in charging of the pillars with neutrality assured by the interstitial substrate [4]. In the upper inset of the same image we also show a SEM image of a single pillar. The eigenmodes of the resonator array are periodic Bloch waves, with charges oscillating between the pillars and the substrate in between, whose dispersion ω_q^{m} is derived in the Supplemental Material [33] following the methods of Yariv [34]. This is illustrated in Fig. 1(b) for a selection of periodicities. In Fig. 1(c) a SEM image of the sample is shown.

As the folded dispersion of the surface phonon polaritons eventually intersect the almost dispersionless localized monopolar mode, we expect the two modes to interact. We can thus exploit the quantum formalism usually employed to describe strongly coupled polaritons [35,36]. Introducing a phenomenological Rabi frequency g_0 coupling the two modes, which in a classical electromagnetic approach would describe the overlap between the surface and monopolar modes, we can describe the coupled system, in the rotating wave approximation, by the Hamiltonian

$$\mathcal{H} = \sum_q \hbar\omega_q^{\mathrm{m}} \hat{a}_q^\dagger \hat{a}_q + \hbar\omega_q^{\mathrm{s}} \hat{b}_q^\dagger \hat{b}_q + \hbar g_0 (\hat{a}_q^\dagger \hat{b}_q + \hat{a}_q \hat{b}_q^\dagger), \quad (2)$$

where $\hat{a}_q$ and $\hat{b}_q$ are the bosonic creation operators for the monopolar modes and surface modes, respectively. As detailed in the Supplemental Material [33], the Hamiltonian in Eq. (2) can be diagonalized by a Hopfield-Bogoliubov procedure [37] in terms of two free normal modes, whose annihilation operators read

$$\hat{p}_q^+ = X_q \hat{a}_q + Y_q \hat{b}_q, \qquad \hat{p}_q^- = Y_q \hat{a}_q - X_q \hat{b}_q, \quad (3)$$

where X_q and Y_q are the Hopfield coefficients describing the mixing of surface and localized modes and the frequency of the normal modes is

$$\omega_q^{\pm} = \frac{\omega_q^{\mathrm{m}} + \omega_q^{\mathrm{s}} \pm \sqrt{(\omega_q^{\mathrm{m}} - \omega_q^{\mathrm{s}})^2 + 4g_0^2}}{2}. \quad (4)$$

The simulated electric field norm for a mode of the coupled system is shown in Fig. 1(d), where for comparison, and in order to highlight the subwavelength character of the coupling, we explicitly show a typical wavelength for the resonant surface mode. A typical dispersion of the normal modes, from Eq. (4), is shown by the dot-dashed lines in Fig. 2(a), in which it is clear how the coupling between localized and surface modes leads to an anticrossing in the dispersion of the normal modes. Fabricated arrays were measured by FTIR microscopy in reflectance mode utilizing a grazing incidence objective. The objective illuminates directionally and the sample is aligned so the peak incident intensity is along the principal axis of the resonator array. Details of the measurement are given in the Supplemental Material [33]. High-angle illumination is achieved by use of a mirror to rotate the incident beam onto the sample resulting in a dual peaked angular excitation as

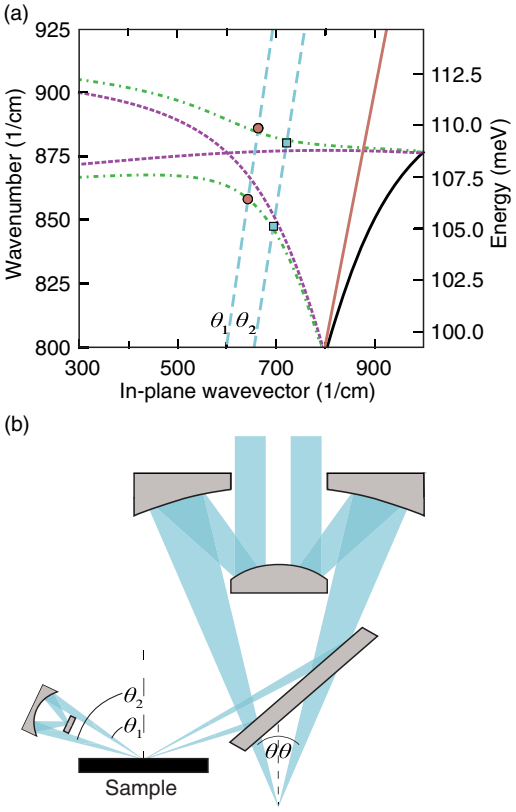

FIG. 2. (a) Dispersion for array period 6.25 μm and coupling constant $g_0 = 1.63$ meV (13.1/cm). Purple dotted lines are the constituent monopolar and folded surface phonon polariton branch, coupled normal modes are green dash-dotted lines. Blue dashed lines represent the two different angles θ_1 and θ_2 sampled by the dual illumination. Squares and circles are the fitted data points from the reflectance plots in the Supplemental Material [33]. (b) Illustration of the function of the grazing incidence objective. A Schwarzschild light path is indicated by angularly symmetric blue rays. The plane mirror at the bottom breaks the cylindrical symmetry of the objective rotating the light cone, initially at an incidence angle θ, toward the sample. After reflecting upon the sample surface the beams strike a spherical mirror and are refocussed on the same spot before passing back into the objective. This results in a dual non-normal double-pass illumination at angles θ_1 and θ_2. Notice that the separation between the two rays is exaggerated here for clarity purpose. The actual data for both the rays' incidence angles and their angular spread can be found in the Supplemental Material [33].

illustrated in Fig. 2(b). This allows two slices of the polariton dispersion to be measured simultaneously as shown in Fig. 2(a). Note that we have until now neglected losses in our theoretical treatment, on account of the large quality factors of both localized and surface phonon polaritons. Still, it is important to remember that the anticrossing shown in Fig. 2(a) is present only if the Rabi frequency g_0 is larger than the losses of both modes, including pure dephasing [11], a condition usually referred to as strong coupling regime. Observing an anticrossing in the system spectrum thus unequivocally proves that energy can be reversibly and coherently exchanged between the two modes, fulfilling the main requirements to use them as building blocks for coherent circuit architectures [12]. The experimental reflectance map we obtained is given in Fig. 3(a) as a function of the array period, that is tuning the surface mode resonance. The data exhibit a clear anticrossing when the two modes are resonant, showing that the system is indeed in the strong coupling regime. Peak positions were then extracted from the experimental reflectance map, clearly highlighting the presence of peaks from two different angles, not apparent in Fig. 3(a) due to the small angular shift and finite linewidth. Individual spectra measured for each array period, and the relative calculated fits can be found in the Supplemental Material [33]. The data was then fitted, following the procedure detailed in the Supplemental Material [33], to the normal mode dispersion given in Eq. (4). The phenomenological coupling g_0 was assumed to vary superradiantly with the in-plane resonator density analogously to scalings in systems where surface plasmons interact with molecular excitons, where in our case the resonators act as effective molecules [38]. The peak positions extracted from the experimental data and the resulting fits are given in Fig. 3(b), where we explicitly show the dispersions at the two different angles. The model reproduces well the anticrossing, within errors of the order of 1 meV (8/cm), a similar magnitude to those reported in previous simulations using finite element modeling [4]. Those errors have been attributed to modifications of the dielectric properties of SiC near the surface due to the strain induced in SiC grown on Si substrates due to the mismatch of lattice parameters [39]. In order to verify this hypothesis we repeated the fitting procedure using the high and low frequency values of the dielectric constants and the TO phonon frequency as additional fit parameters. The resulting values for the dielectric parameters differ less than 5% from the standard values found in the literature [19] and the TO phonon shifts just 0.74 meV (6.1/cm), but they lead to a dramatic improvement of the fits, shown in Fig. 3(c). The maximal value of the fitted Rabi frequency is $g_0 = 2.55$ meV (20.6/cm), leading to a ratio between g_0 and the bare frequency of the excitation of the order of 10^{-2}, thus justifying *a posteriori* the rotating wave approximation we used in Eq. (2) [40]. We also extracted the linewidths of the different normal modes from the reflectance map, and we were able to fit them assuming they are sums of the

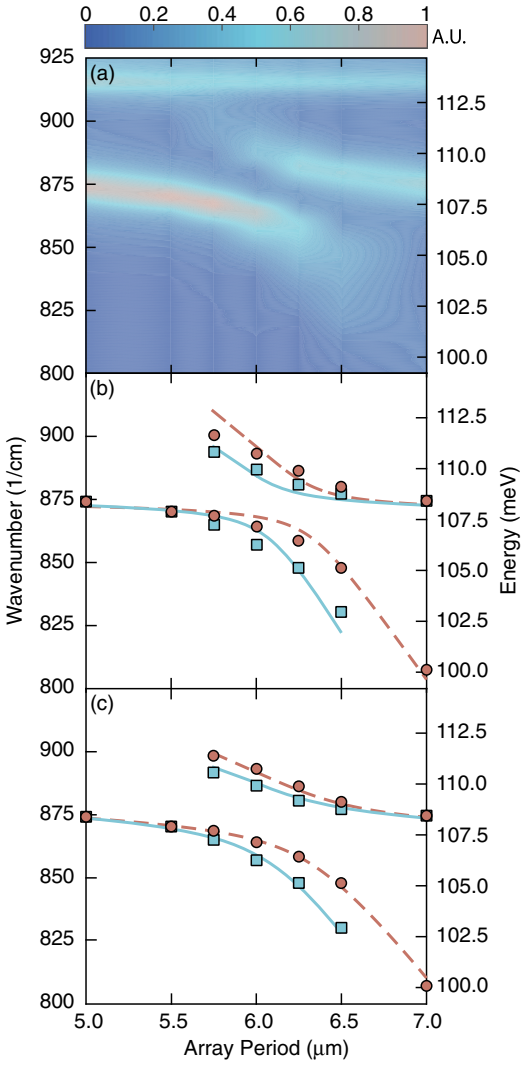

FIG. 3. The top panel (a) shows the background subtracted experimental reflectance map of SiC cylinder arrays of varying period. The almost dispersionless mode at 113.75 meV (917.4/cm) is the transverse dipole resonance discussed elsewhere [4]. The peaks extracted from the reflectance map are given in the lower panels for the larger angle by blue squares and the smaller by red circles. Solid blue lines and dashed red lines are the corresponding fits, enacted using book values for the dielectric constants of SiC (b) [19], or fitting also the dielectric constants of SiC (c) as free parameters.

constituents' ones, weighted by the relative Hopfield coefficients [41]. We found linewidths at the anticrossing of the order of 1 meV (8/cm). In the densest array we considered, energy is thus coherently transferred between monopolar and surface modes roughly 4 times before escaping. More details, including the extracted experimental linewidths, can be found in the Supplemental Material [33].

In summary, we have demonstrated that, exploiting the tunability of surface phonon polaritons dispersion, it is possible to observe a clear spectral anticrossing between localized and surface phonon polaritons, proving that

coherent, reversible energy exchange is possible between them. In combination with the high confinements and Purcell enhancements recently observed in user-defined structures, the present Letter takes a decisive step in demonstrating the versatility and tunability of phonon polaritons for coherent applications in the midinfrared spectral region. In particular, the coherent interplay between localized and propagative, nonradiative modes, together with the relatively large quality factors achievable in those systems, could make it possible to design quantum architectures similar to quantum plasmonic circuits, but without many of the limitations due to plasmon intrinsic losses.

F. M. and A. P. thank the Southampton Nanofabrication Centre staff for technical support, S. A. M. acknowledges support from EPSRC programme Grants No. EP/L024926/1 and No. EP/M013812/1, plus ONR Global, the EOARD, the Royal Society, and the Lee-Lucas Chair in Physics. S. D. L. is a Royal Society Research Fellow and he acknowledges support from EPSRC Grant No. EP/M003183/1.

[1] G. Borstel, H. J. Falge, and A. Otto, Surface and bulk phonon-polaritons observed by attenuated total reflection, Springer Tracts Mod. Phys. **74**, 107 (1974).
[2] J. D. Caldwell, L. Lindsay, V. Giannini, I. Vurgaftman, T. L. Reinecke, S. A. Maier, and O. J. Glembocki, Low-loss, infrared and terahertz nanophotonics using surface phonon polaritons, Nanophotonics **4**, 44 (2015).
[3] J. A. Schuller, T. Taubner, and M. L. Brongersma, Optical antenna thermal emitters, Nat. Photonics **3**, 658 (2009).
[4] J. D. Caldwell, O. J. Glembocki, Y. Francescato, N. Sharac, V. Giannini, F. J. Bezares, J. P. Long, J. C. Owrutsky, I. Vurgaftman, J. G. Tischler, V. D. Wheeler, N. D. Bassim, L. M. Shirley, R. Kasica, and S. A. Maier, Low-loss, extreme subdiffraction photon confinement via silicon carbide localized surface phonon polariton resonators, Nano Lett. **13**, 3690 (2013).
[5] J. Le Gall, M. Olivier, and J.-J. Greffet, Experimental and theoretical study of reflection and coherent thermal emission by a SiC grating supporting a surface-phonon polariton, Phys. Rev. B **55**, 10105 (1997).
[6] A. Huber, N. Ocelic, D. Kazantsev, and R. Hillenbrand, Near-field imaging of mid-infrared surface phonon polariton propagation, Appl. Phys. Lett. **87**, 081103 (2005).
[7] G. Di Martino, Y. Sonnefraud, S. Kéna-Cohen, M. Tame, Ş. K. Özdemir, M. S. Kim, and S. A. Maier, Quantum Statistics of Surface Plasmon Polaritons in Metallic Stripe Waveguides, Nano Lett. **12**, 2504 (2012).
[8] G. Fujii, T. Segawa, S. Mori, N. Namekata, D. Fukada, and S. Inoue, Preservation of photon indistinguishability after transmission through surface-plasmon-polariton waveguide, Opt. Lett. **37**, 1535 (2012).
[9] R. W. Heeres, L. P. Kouwenhoven, and V. Zwiller, Quantum interference in plasmonic circuits, Nat. Nanotechnol. **8**, 719 (2013).
[10] N. P. de Leon, M. D. Lukin, and H. Park, Quantum plasmonic circuits, IEEE J. Sel. Top. Quantum Electron. **18**, 1781 (2012).
[11] A. Auffèves, D. Gerace, J. M. Gèrard, M. Franca Santos, L. C. Andreani, and J. P. Poizat, Controlling the dynamics of a coupled atom-cavity system by pure dephasing, Phys. Rev. B **81**, 245419 (2010).
[12] A. Konrad, A. M. Kern, M. Brecht, and A. J. Meixner, Strong and coherent coupling of a plasmonic nanoparticle to a subwavelength Fabry Pérot resonator, Nano Lett. **15**, 4423 (2015).
[13] S. A. Maier, *Plasmonics: Fundamentals and Applications* (Springer, New York, 2007).
[14] J. Takahara, S. Yamagishi, H. Taki, A. Morimoto, and T. Kobayashi, Guiding of a one-dimensional optical beam with nanometer diameter, Opt. Lett. **22**, 475 (1997).
[15] S. Schlücker, Surface-enhanced Raman spectroscopy: concepts and chemical applications, Angew. Chem. Int. Ed **53**, 4756 (2014).
[16] J. B. Khurgin, How to deal with the loss in plasmonics and metamaterials, Nat. Nanotechnol. **10**, 2 (2015).
[17] J. B. Khurgin and G. Sun, Scaling of losses with size and wavelength in nanoplasmonics and metamaterials, Appl. Phys. Lett. **99**, 211106 (2011).
[18] M. S. Tame, K. R. McEnergy, S. K. Özdemir, J. Lee, S. A. Maier, and M. S. Kim, Quantum plasmonics, Nat. Phys. **9**, 329 (2013).
[19] K. M. Pitman, A. M. Hofmeister, A. B. Corman, and A. K. Speck, Optical properties of silicon carbide for astrophysical applications, Astron. Astrophys. **483**, 661 (2008).
[20] S. Shen, A. Narayanaswamy, and G. Chen, Surface phonon polaritons mediated energy transfer between nanoscale gaps, Nano Lett. **9**, 2909 (2009).
[21] S. A. Holmstrom, T. H. Stievater, M. W. Pruessner, D. Park, W. S. Rabinovich, J. B. Khurgin, C. J. K. Richardson, S. Kanakaraju, L. C. Calhoun, and R. Ghodssi, Guided-mode phonon-polaritons in suspended waveguides, Phys. Rev. B **86**, 165120 (2012).
[22] J.-J. Greffet, R. Carminati, K. Joulain, J.-P. Mulet, S. Mainguy, and Y. Chen, Coherent emission of light by thermal sources, Nature (London) **416**, 61 (2002).
[23] N. Dahan, A. Niv, G. Biener, V. Kleiner, and E. Hasman, Space-variant polarization manipulation of a thermal emission by a SiO_2 subwavelength grating supporting surface phonon-polaritons, Appl. Phys. Lett. **86**, 191102 (2005).
[24] T. Taubner, D. Korobkin, Y. Urzhumov, G. Shvets, and R. Hillenbrand, Near-field microscopy through a SiC superlens, Science **313**, 1595 (2006).
[25] S. C. Kehr, Y. M. Liu, L. W. Martin, P. Yu, M. Gajek, S.-Y. Yang, C.-H. Yang, M. T. Wenzel, R. Jacob, H.-G. von Ribbeck, M. Helm, X. Zhang, L. M. Eng, and R. Ramesh, Near-field examination of perovskite-based superlenses and superlens-enhanced probe-object coupling, Nat. Commun. **2**, 249 (2011).
[26] T. Taubner, F. Keilmann, and R. Hillenbrand, Nanomechanical resonance tuning and phase effects in optical near-field interaction, Nano Lett. **4**, 1669 (2004).
[27] D. Li, N. M. Lawandy, and R. Zia, Surface phonon-polariton enhanced optical forces in silicon carbide nanostructures, Opt. Express **21**, 20900 (2013).

[28] R. Hillenbrand, T. Taubner, and F. Keilmann, Phonon-enhanced light-matter interaction at the nanometre scale, Nature (London) **418**, 159 (2002).

[29] J. D. Caldwell, A. V. Kretinin, Y. Chen, V. Giannini, M. M. Fogler, Y. Francescato, C. T. Ellis, J. G. Tischler, C. R. Woods, A. J. Giles, M. Hong, K. Watanabe, T. Taniguchi, S. A. Maier, and K. S. Novoselov, Sub-diffractional volume-confined polaritons in the natural hyperbolic material hexagonal boron nitride, Nat. Commun. **5**, 5221 (2014).

[30] H. Mutschke, A. C. Andersen, D. Clement, T. Henning, and G. Peiter, Infrared properties of SiC particles, Astron. Astrophys. **345**, 187 (1999).

[31] Y. Chen, Y. Francescato, J. D. Caldwell, V. Giannini, T. W. W. Maß, O. J. Glembocki, F. J. Bezares, T. Taubner, R. Kasica, M. Hong, and S. A. Maier, Spectral tuning of localized Surface Phonon polariton Resonators for low-loss mid-IR applications, ACS Photonics **1**, 718 (2014).

[32] M.-K. Kim, H. Sim, S. J. Yoon, S.-H. Gong, C. W. Ahn, Y.-H. Cho, and Y.-H. Lee, Squeezing Photons into a Point-Like Space, Nano Lett. **15**, 4102 (2015).

[33] See Supplemental Material at http://link.aps.org/supplemental/10.1103/PhysRevLett.116.246402 for details on fabrication, measurements and data analysis.

[34] A. Yariv, Y. Xu, R. K. Lee, and A. Scherer, Coupled-resonator optical waveguide: A proposal and analysis, Opt. Lett. **24**, 711 (1999).

[35] J. J. Hopfield, Theory of the Contribution of Excitons to the Complex Dielectric Constant of Crystals, Phys. Rev. **112**, 1555 (1958).

[36] V. Savona, Z. Hradil, A. Quattropani, and P. Schwendimann, Quantum theory of quantum-well polaritons in semiconductor microcavities, Phys. Rev. B **49**, 8774 (1994).

[37] Y. Todorov, Dipolar quantum electrodynamics theory of the three-dimensional electron gas, Phys. Rev. B **89**, 075115 (2014).

[38] N. I. Cade, T. Ritman-Meer, and D. Richards, Strong coupling of localized plasmons and molecular excitons in nanostructured silver films, Phys. Rev. B **79**, 241404 (2009).

[39] G. Ferro, T. Chassagne, A. Leycuras, F. Cauwet, and Y. Monteil, Strain tailoring in 3C-SiC heteroepitaxial layers grown on Si(100), Chem. Vap. Deposition **12**, 483 (2006).

[40] A. A. Anappara, S. De Liberato, A. Tredicucci, C. Ciuti, G. Biasiol, L. Sorba, and F. Beltram, Signatures of light-matter excitations in the ultra-strong coupling regime, Phys. Rev. B **79**, 201303(R) (2009).

[41] S. De Liberato, Light-Matter Decoupling in the Deep Strong Coupling Regime: The Breakdown of the Purcell Effect, Phys. Rev. Lett. **112**, 016401 (2014).